applied optics

Simple and robust algorithm to extend the dynamic range of tip-tilt for a Shack–Hartmann sensor

Mingxing Li,[1,2] Dayu Li,[1] Lifa Hu,[1] Quanquan Mu,[1] Zhaoliang Cao,[1] Huanyu Xu,[1] Xinghai Lu,[1] and Li Xuan[1,*]

[1]State Key Laboratory of Applied Optics, Changchun Institute of Optics, Fine Mechanics and Physics, Chinese Academy of Sciences, Changchun 130033, China
[2]University of Chinese Academy of Sciences, Beijing 100039, China
*Corresponding author: xuanli1957@sina.com

Received 22 April 2015; revised 29 June 2015; accepted 23 September 2015; posted 23 September 2015 (Doc. ID 238472); published 20 October 2015

We propose an algorithm to extend the dynamic range of tip-tilt (TT) for a Shack–Hartmann wave-front sensor. With this method, the dynamic range of TT is determined by the size of the whole CCD pixel array rather than the size of the sub-aperture. Thus the separate TT sensor in adaptive optics (AO) systems for optical telescope can be saved, which will simplify the systems and enhance the light energy efficiency. The proposed algorithm is computationally effective and appropriate for the real-time TT computation of AO systems. The simulated and experimental results show that the algorithm is robust to realistic scintillation and photon noise and can work well under poor observing conditions. For the given condition with r_0 of 5 cm at 550 nm and average flux of 100 photons per sub-aperture, the ultimate measurement accuracy of TT is about 5% pixels (peak-to-valley value).

OCIS codes: (010.1080) Active or adaptive optics; (010.1290) Atmospheric optics; (010.7350) Wave-front sensing.

http://dx.doi.org/10.1364/AO.54.009030

1. INTRODUCTION

Shack–Hartmann based Adaptive Optics (AO) system has been widely used in large ground-based telescopes to compensate atmospheric turbulence and telescope aberrations [1–3]. The detection of tip-tilt (TT) aberrations is important for AO systems because compensating them alone can significantly improve the quality of an image [4]. In the case of laser beacon AO systems, a separate TT sensor is essential, because a beacon launched from the ground cannot function as an absolute position reference and a different object is needed for the TT sensing [2]. When the science object itself or a nearby star functions as the reference, the TT information can be extracted from the Shack–Hartmann wave-front sensor (SHWFS), so a separate TT sensor is not necessary. However, when the amount of TT aberrations is too large due to the vibration and tracking error of the telescope [5,6], and the amplitude of residual TT aberrations appear on the SHWFS is over the dynamic range of SHWFS before closing the TT loop, a separate TT sensor with lower accuracy but larger dynamic range is required. The rough TT tracking signals obtained from the separate TT sensor are used to drive the TT corrector conjugated to the SHWFS to decrease the residual TT aberrations until all SHWFS spots return to the FOV of their lenslets. Then the average of centroid biases of all valid spots will be used for fine TT tracking [7].

However, if the dynamic range of TT for the SHWFS is large enough, the separate TT sensor can be saved, which will simplify the AO system and enhance light energy efficiency. Many methods are proposed to extend the dynamic range of the SHWFS, such as using astigmatic lenslets [8] or a spatial light modulator array [9], iterative extrapolation methods [10,11] and modified unwrapping algorithms [12]. But the dynamic range of TT with these methods is still smaller than one sub-aperture. Furthermore, they are usually complicated and time-consuming and cannot be used in the real-time AO correction. In this paper, we propose a simple and robust algorithm based on the grid meshing [13] and template matching to enlarge the dynamic range of TT. The algorithm can identify the spots by grid meshing and retrieve the corresponding lenslet of each spot by template matching. With our method, the dynamic range of TT will be determined by the size of the whole CCD pixel array rather than the size of the sub-aperture.

The remainder of the paper is as follows: The detailed algorithm is given in Section 2. In Section 3 the simulated SHWFS

spots corrupted by realistic scintillation (not weak) [14,15] and photon noise [16] are used to verify the efficiency of our algorithm. This is followed by experimental results in Section 4, and conclusions are drawn in Section 5.

2. DETAIL OF THE ALGORITHM

The algorithm proposed in this paper consists of two steps: identifying the spots and retrieving the corresponding lenslet of each spot.

Assume that all spots stay in the FOV of their lenslets when the amount of TT is very small, as shown in Fig. 1(a). The grid pattern identifies all spots and the centroid position of each spot can be calculated using the CCD signals in its corresponding grid. When large-amplitude TT aberrations appear on the SHWFS, all spots will be biased consistently as in Fig. 1(b). The spots on the CCD cannot be identified using the original grid pattern anymore. This can be solved by shifting the original grid pattern as in Fig. 2(a). The principle of horizontal shift is locating each column of spots near the center of two adjacent vertical grid lines as far as possible. The horizontal center of each column of spots can be calculated by the mean gray level of each vertical line of SHWFS spots. And the horizontal displacement can be obtained from these horizontal centers. Using the same method, the vertical displacement of the grid pattern can be computed as well. After locating the grid pattern, each grid corresponds to a subzone, and we can easily get the centroid position of spot in each subzone.

The next step is finding the lenslet that corresponds to each measured centroid position, which can be solved with the template matching method:

$$C(m, n) = \sum_{p,q} S(p, q)M(p - m, q - n). \quad (1)$$

$S(p, q)$ is the total intensity of the spot in the (p, q) subzone, and the total intensity map is illustrated in Fig. 2(b). $M(p - m, q - n)$ represent the geometry matrixes after translations and Fig. 3 gives some examples of them. C is the total intensity of all valid spots. Once the maximum index (m, n) of C is found, the matching is achieved: the spot in (p, q) subzone is corresponding to the $(p - m, q - n)$ lenslet. For the grid pattern shown in Fig. 2(a), the maximum index of C should be (1, 1), and its corresponding geometry matrix is shown as Fig. 3(f). Given that each lenslet is associated with a reference

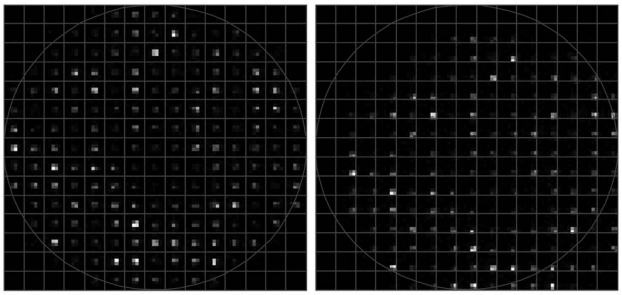

Fig. 1. (a) The SHWFS spots stay in the FOV of their lenslets when the amount of TT aberrations is very small. (b) All spots leave the FOV of their lenslets due to the large-amplitude TT.

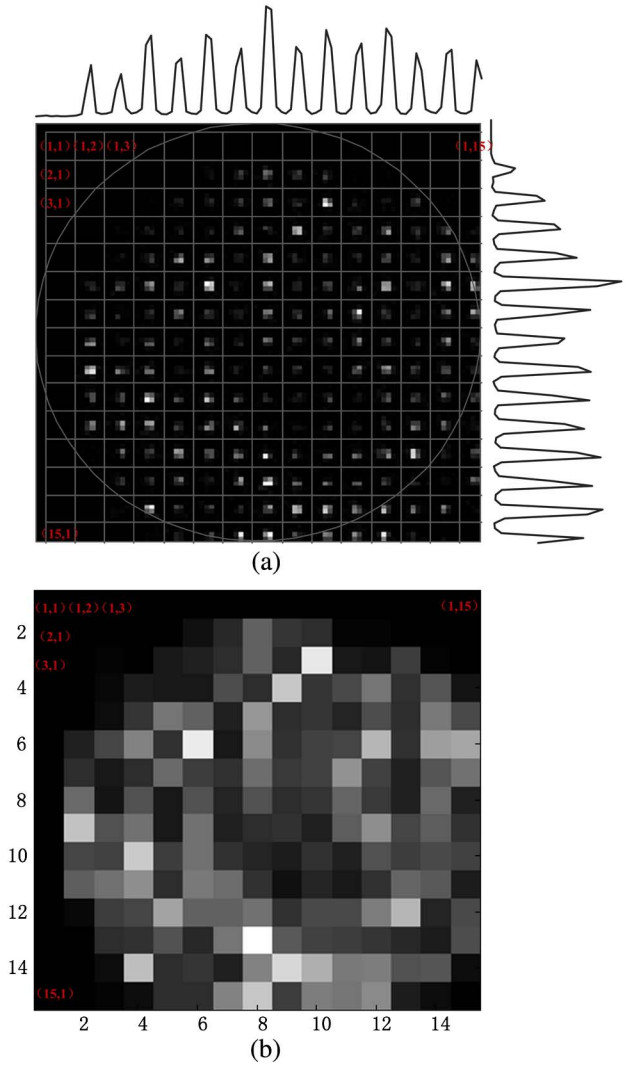

Fig. 2. (a) The curve above (or on the right of) the spots pattern means the mean gray level of each vertical (or horizontal) line of the SHWFS spots. The spots are identified by the grid pattern after translations. (b) Total intensity map: each gray value means the total intensity of the spot in its corresponding subzone.

position in the pupil plane, it is easy to obtain the centroid bias of each spot and decide whether it is valid. Thus the TT signals can be estimated by calculating the average of centroid biases of all valid spots whether the spots stay in the FOV of their lenslets or not.

If the CCD pixel array is large enough, the spots will not be lost due to the large-amplitude TT and the relation between the measured centroid positions and their lenslets can be retrieved correctly with the template matching method. However, considering the readout speed and the utilization rate of devices, the CCD pixel array should be as small as possible. Thus when the large-amplitude TT aberrations appear on the SHWFS some spots will lost, which will affect the retrieving of the relation between the centroid positions and their lenslets. For example, if the mark of geometry matrix in Fig. 3(p) is white, the mark in the same position of that in Fig. 3(k) is also white. That is to say, if both the tip (x-direction) and tilt

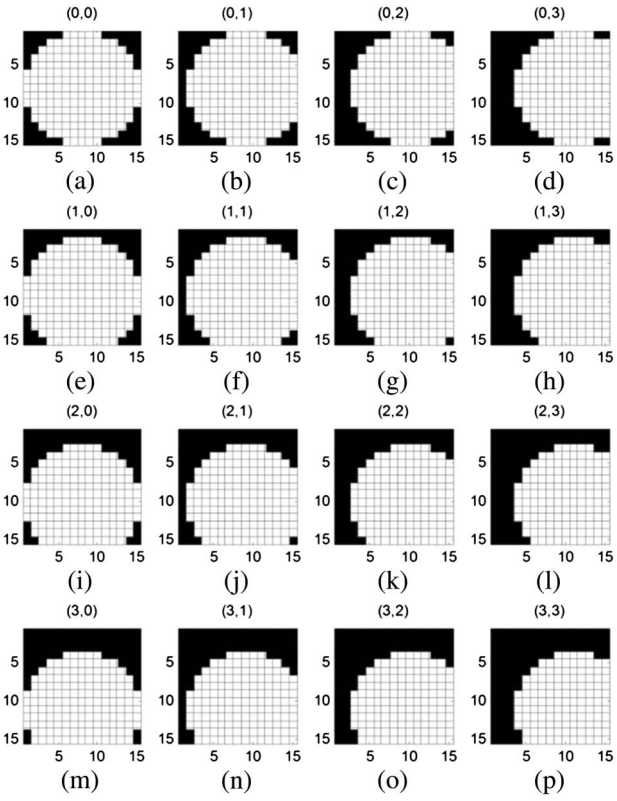

Fig. 3. Examples of geometry matrixes after translations. The white mark means that the spot in this subzone is valid. The title of each sub-graph indicates the amount of movement for the geometry matrix.

(y-direction) are three sub-apertures, the corresponding geometry matrix found by our method may be one of the sub-graphs as depicted in Figs. 3(k) and 3(p), while only the one depicted in Fig. 3(p) is the right answer. Fortunately, either of them is regarded as the corresponding geometry matrix, the measurements can be used to drive the TT corrector to decrease the residual TT aberrations. For the SHWFS with hexagonal configuration, the method is also applicable. We give the spots pattern formed by a SHWFS with hexagonal configuration and its corresponding geometry matrix in Fig. 4.

3. SIMULATION

In order to verify the efficiency and practicability of our algorithm, we simulated the SHWFS spots corrupted by realistic scintillation and photon noise. First, we generated random atmospheric turbulence phase screens with Kolmogorov statistics using Fourier method [17]. The large complex light amplitude screens at the telescope pupil were generated by the propagation through a single turbulent layer with r_0 value of 5 cm at 550 nm located above the ground 4 km. The propagation of wave-fronts was achieved by the spectral technique [15]:

$$V_1(f) = F\{U_1(r)\}, \tag{2}$$

$$V_2(f) = V_1(f)\ \exp(-i\pi\lambda z|f|^2), \tag{3}$$

$$U_2(r) = F^{-1}\{V_2(f)\}, \tag{4}$$

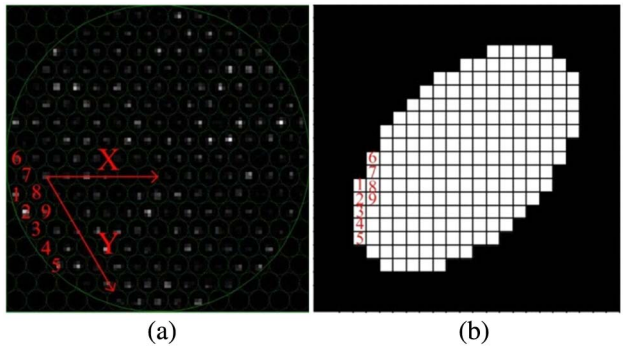

Fig. 4. (a) Spots pattern formed by a SHWFS with hexagonal configuration. (b) Geometry matrix of the SHWFS. The red numbers show the correspondences between the lenslets and the geometry matrix. When the spots pattern moves by one sub-aperture along the x-direction (the spot in subzone marked by the "1" moves to the subzone marked by the "8"), its corresponding geometry matrix should move by one grid to right. If the spots pattern moves by one sub-aperture along the y-direction (the spot in subzone marked by the "1" moves to the subzone marked by the "2"), its corresponding geometry matrix should move by one grid down.

where $U_1(r)$ and $U_2(r)$ are the complex amplitude of the light before and after propagation over a distance z, respectively, F denotes the Fourier transform and F^{-1} the inverse Fourier transform. Figure 5(a) gives an example of simulated scintillation screens. The pupil magnification of the telescope pupil to the SHWFS is 174:1. The detail parameters of the SHWFS given in Table 1 are used throughout this paper. The complex light amplitude after pupil zooming was then sampled by the lenslet array of the SHWFS, which produced an array of spots on the CCD, as shown in Fig. 5(b). After that, light intensity in each

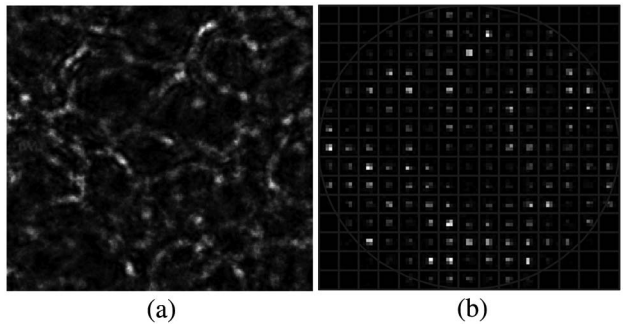

Fig. 5. (a) Example of relative irradiance screen of 1 m^2 size. (b) Simulated SHWFS spots pattern corrupted by realistic scintillation and photon noise.

Table 1. Detail Parameters of SHWFSs

Parameter	Value
Diameter of the pupil	4.32 mm
Size of the lenslet	288 μm
Focal length of the lenslet	19.35 mm
Pixel number of each sub-aperture	6 * 6
Pixel size	48 μm

detector pixel was corrupted by the photon noise (following Poisson statistics) and the average photon number per spot per frame is 100. To simulate the data sequence of SHWFS, the screens were shifted in both coordinates by vt, the wind speed v and time sampling interval t were 20 m/s and 1 ms, respectively. Note that we can adjust the TT aberrations by adding additional TT in the simulations.

Figure 6 shows some examples of simulated SHWFS spots with different TT aberrations and grid patterns after translations with our method. It can be seen that the grid patterns after translations can identify the spots correctly. The centroid of each spot can be obtained by using the CCD signals in its corresponding grid. Note that we computed the centroid of each spot using the center-of-gravity algorithm [16] in this paper. The simulated results are illustrated in Fig. 7. For the TT aberrations with certain amplitudes, 1000 frames of SHWFS spots were measured. We can see that there exists excellent agreement between the measured values with our method and the theoretical values when the displacement of spots pattern is less than 12 pixels (2 sub-apertures). When the displacement of the spots pattern is greater than 12 pixels, the serious loss of spots leads to the unsuccessful matching between the spots and their lenslets, and the measurement accuracy of our algorithm decreases sharply. Although the measured values are far less than the theoretical values, they are always greater than 5 pixels. That is to say, the SHWFS spots can return the FOV of their lenslets as in Fig. 5(b) after dozens of closed-loop TT corrections even though both the initial tip and tilt are 50 pixels as in Fig. 6(b).

When a large number of spots move outside of the CCD, there is a more suitable method to decrease the residual TT aberrations faster. We assume that the spots pattern is a disk with uniform luminance as shown in Fig. 8(a). "+" is the average centroid position of the spots on the CCD and "Δ" is the theoretical centroid position of the spots pattern. The relationship between the average centroid bias of the spots on the CCD and the theoretical centroid bias of the spots pattern is shown in Fig. 8(b). So the TT signals can be obtained based on this relationship once the average center of spots on the CCD is estimated. Figure 9 gives the iterations of closing the TT loop for the two methods. Both the initial tip and tilt are 50 pixels and the TT mirror has the ideal response. It can be seen from the curve diagrams that with the method based on grid meshing and template matching the TT loop can be closed after 5–6 iterations. While for the method shown in Fig. 8, the residual TT will decrease sharply although the TT loop can't be closed due to realistic scintillation and photon noise. So, the TT loop will be closed faster by using the combination of the two methods. By the way, the switch between the two methods becomes easier due to their large dynamic range of TT.

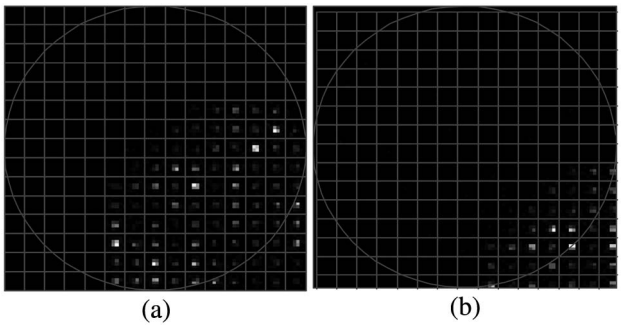

Fig. 6. Simulated SHWFS spots patterns with different TT aberrations. Both the tip and tilt are: (a) 30 pixels and (b) 50 pixels.

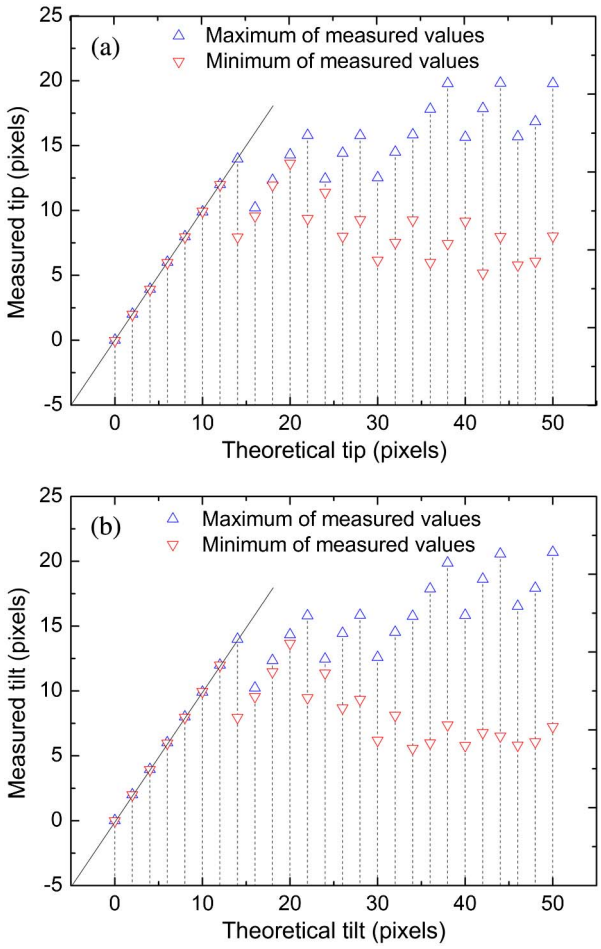

Fig. 7. Comparison of the measured TT from our method with the theoretical TT for the SHWFS with square configuration: (a) tip values and (b) tilt values. The theoretical tip and tilt are equal. The solid lines indicate that the measured values are equal to the theoretical values. The measurement error is about 5% pixels (peak-to-valley value) when all spots stay in the FOV of their lenslets.

Besides, we used simulated spots to verify the efficiency of our method for the SHWFS with hexagonal configuration. The simulation results are illustrated in Fig. 10. From the measuring results from Figs. 7 and 10, we can see that only the geometry matrixes with small displacements (less than 4 grids) are useful. In other words, just using these geometry matrixes, the TT tracking can be accomplished with our method. For these geometry matrixes, the number of valid spots on the CCD is much larger than that of invalid spots. So we can set $M(p-m, q-n)$ in Eq. (1) to 0 if the spot in $(p-m, q-n)$ subzone is valid, otherwise 1, and then find the minimum of C to accomplish the template matching. This will reduce the calculations. Using a computer with the Inter Core (TM) i5-3550 3.3 GHz and a C++ implementation of the optimized algorithm, the full

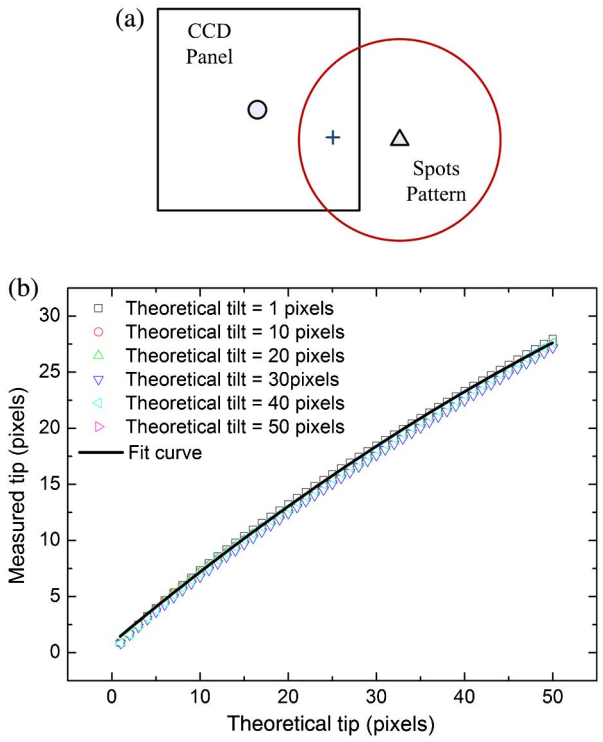

Fig. 8. (a) A large number of spots move outside of the CCD due to large-amplitude TT aberrations. "○" is the reference position. "△" is the theoretical centroid position of the spots pattern. "+" is the average centroid position of the spots on the CCD. (b) The relationship between the measured and theoretical TT values is: $Y = 0.68 + 0.66X - 0.0025 \times 2$, where X represents the theoretical centroid bias of the spots pattern and Y stands for the average centroid bias of the spots on the CCD.

process takes approximatively 50 μs including 30 μs for computing the centroid position of all spots. So the method is applicable for the real-time TT computation of AO systems especially for the observations of high-speed objects, in which

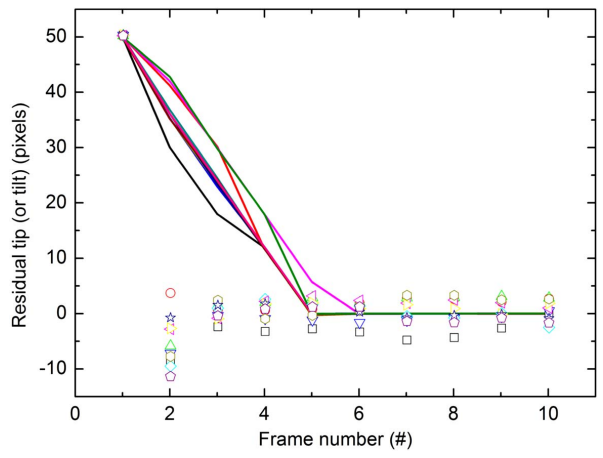

Fig. 9. Iterations of closing the TT loop for five different turbulence series. Both the initial tip and tilt are 50 pixels and the TT mirror has the ideal response. The curves diagrams represent the results for the method based on grid meshing and template matching, while the results of the method shown in Fig. 8 are depicted by the scatters diagrams.

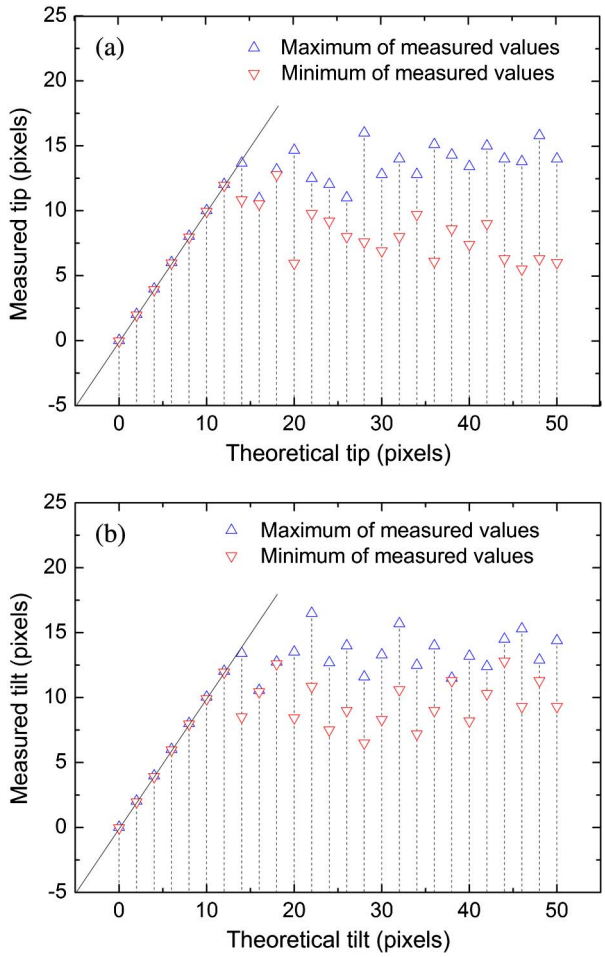

Fig. 10. Measured TT for the SHWFS with hexagonal configuration: (a) tip values and (b) tilt values.

case the method has to be used all the time to monitor whether the SHWFS spots move outside the FOV of their lenslets and provide TT signals to TT corrector to drive the spots to their subzones as soon as possible.

4. EXPERIMENT

We also used the experimental SHWFS spots to verify the efficiency of our algorithm. The system layout shown in Fig. 11 was used in the experiment. Both the TT mirror and the lenslet array of SHWFS are conjugated to the pupil plane. The random turbulence phase screens with Kolmogorov statistics were generated by the turbulence simulator. The turbulence simulator was not located at the pupil plane "P", which produced realistic scintillation. The TT mirror is used to simulate the vibration and tracking error of the telescope and the amount of TT aberrations that appear on the SHWFS can be adjusted by it. The average photon number per spot per frame is about 200 rather than 100 because of the multiple amplification stages for electron multiplication CCDs [16]. Figure 12 shows some examples of the experimental SHWFS spots. Note that in the experiment we cannot know the theoretical TT like the numerical simulation. So we first measured the TT aberrations

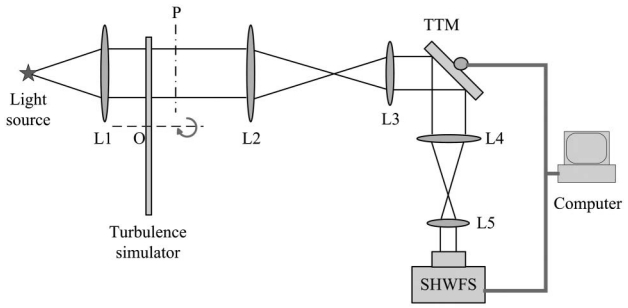

Fig. 11. Sketch of experimental system layout. TTM, tip-tilt mirror; P, pupil plane conjugated with the TTM and the lenslet array of the SHWFS.

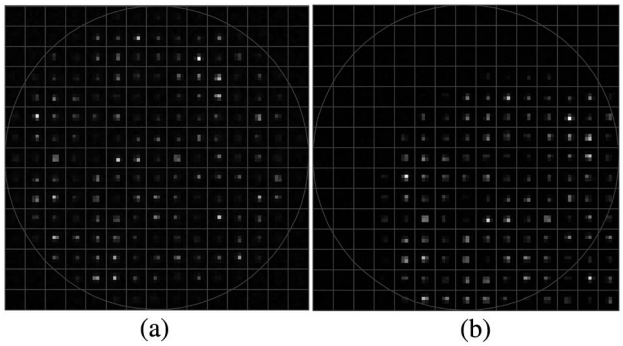

Fig. 12. Experimental SHWFS spots corrupted by realistic scintillation and photon noise.

when all spots stayed in the FOV of their lenslets and the average photon number per spot per frame was very large (high signal-to-noise ratio). Then we added known TT aberrations by the TT mirror and got the SHWFS spots with the known theoretical TT. In the experiment, we generated SHWFS spots patterns by propagation through five different turbulence phase screens. The experimental results shown in Fig. 13 are consistent with the simulated results depicted in Figs. 7 and 10.

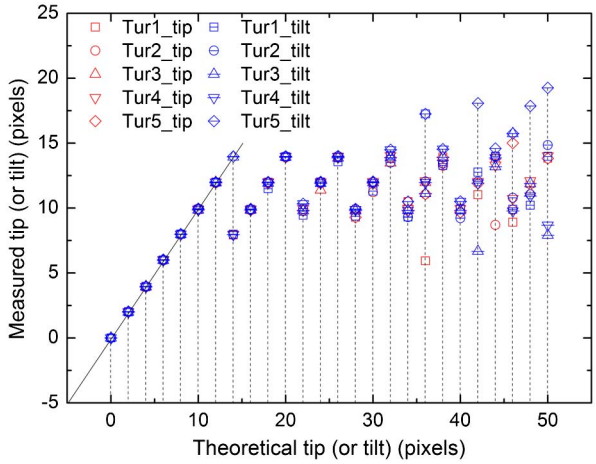

Fig. 13. Measured TT for experimental SHWFS spots.

5. CONCLUSION

We have proposed a simple and effective algorithm based on grid meshing and template matching to significantly extend the dynamic range of TT for a SHWFS. The simulated and experimental results show that the algorithm is robust to realistic scintillation and photon noise and can work well under observing conditions with r_0 of 5 cm at 550 nm and average flux of 100 photons per sub-aperture. When the displacement of SHWFS spots pattern is less than 12 pixels (2 sub-apertures), accurate TT can be got by our algorithm though some spots move outside of the CCD. As the amount of TT becomes greater, the measurement accuracy of our algorithm will decrease due to the serious loss of spots and the unsuccessful matching between the spots and their lenslets. Nevertheless, the measurements (at least 5 pixels) can be used to reduce the residual TT aberrations until the spots return to the FOV of their lenslets. The ultimate measurement error of TT is about 5% pixels (peak-to-valley value). With our method, the dynamic range of TT is determined by the size of the whole CCD pixel array rather than the size of the sub-aperture. Thus the separate TT sensor can be saved, which will simplify the AO systems and enhance the light energy efficiency. Moreover, our method is applicable for SHWFSs with both square and hexagonal configurations. The timing test has also shown that our algorithm is computationally effective and appropriate for the real-time TT computation of AO systems.

Funding. National Natural Science Foundation of China (NSFC) (61205021, 61377032, 61405194, 61475152); Chinese Academy of Sciences (CAS).

REFERENCES

1. D. M. Alloin and J.-M. Mariotti, *Adaptive Optics for Astronomy* (Springer, 1994), Vol. **423**.
2. J. W. Hardy, *Adaptive Optics for Astronomical Telescopes* (Oxford University, 1998).
3. R. Tyson, *Principles of Adaptive Optics* (CRC Press, 2010).
4. H. Babcock, B. Rule, and J. Fassero, "An improved automatic guider," Publ. Astron. Soc. Pac. **68**, 256–258 (1956).
5. X. Ma, K. Wei, W. Zheng, and C. Rao, "A composite tracking sensor with high accuracy and large dynamic range," Proc. SPIE **9148**, 914855 (2014).
6. B. Sedghi, M. Müller, H. Bonnet, M. Dimmler, and B. Bauvir, "Field stabilization (tip/tilt control) of E-ELT," Proc. SPIE **7733**, 773340 (2010).
7. M. A. van Dam, D. Le Mignant, and B. A. Macintosh, "Performance of the Keck Observatory adaptive-optics system," Appl. Opt. **43**, 5458–5467 (2004).
8. N. Lindlein and J. Pfund, "Experimental results for expanding the dynamic range of a Shack-Hartmann sensor using astigmatic microlenses," Opt. Eng. **41**, 529–533 (2002).
9. N. Lindlein, J. Pfund, and J. Schwider, "Algorithm for expanding the dynamic range of a Shack-Hartmann sensor by using a spatial light modulator array," Opt. Eng. **40**, 837–840 (2001).
10. C. Leroux and C. Dainty, "A simple and robust method to extend the dynamic range of an aberrometer," Opt. Express **17**, 19055–19061 (2009).
11. M. Xia, C. Li, L. Hu, Z. Cao, Q. Mu, and L. Xuan, "Shack-Hartmann wavefront sensor with large dynamic range," J. Biomed. Opt. **15**, 026009 (2010).
12. J. Pfund, N. Lindlein, and J. Schwider, "Dynamic range expansion of a Shack-Hartmann sensor by use of a modified unwrapping algorithm," Opt. Lett. **23**, 995–997 (1998).

13. L. A. Carvalho, "A simple and effective algorithm for detection of arbitrary Hartmann-Shack patterns," J. Biomed. Opt. **37**, 1–9 (2004).
14. L. C. Andrews, R. L. Phillips, C. Y. Hopen, and M. Al-Habash, "Theory of optical scintillation," J. Opt. Soc. Am. A **16**, 1417–1429 (1999).
15. A. Tokovinin and V. Kornilov, "Accurate seeing measurements with MASS and DIMM," Mon. Not. R. Astron. Soc. **381**, 1179–1189 (2007).
16. S. Thomas, T. Fusco, A. Tokovinin, M. Nicolle, V. Michau, and G. Rousset, "Comparison of centroid computation algorithms in a Shack-Hartmann sensor," Mon. Not. R. Astron. Soc. **371**, 323–336 (2006).
17. G. Sedmak, "Implementation of fast-Fourier-transform-based simulations of extra-large atmospheric phase and scintillation screens," Appl. Opt. **43**, 4527–4538 (2004).